SANDIA REPORT

SAND2006-7779
Unlimited Release
Printed February 2007

Helium Bubble Linkage and the Transition to Rapid He Release in Aging Pd Tritide

D. F. Cowgill
Analytical Materials Science Dept.

Prepared by
Sandia National Laboratories
Albuquerque, New Mexico 87185 and Livermore, California 94550

Sandia is a multiprogram laboratory operated by Sandia Corporation,
a Lockheed Martin Company, for the United States Department of Energy's
National Nuclear Security Administration under Contract DE-AC04-94-AL85000.

Sandia National Laboratories

Issued by Sandia National Laboratories, operated for the United States Department of Energy by Sandia Corporation.

Available to DOE and DOE contractors from
U.S. Department of Energy
Office of Scientific and Technical Information
P.O. Box 62
Oak Ridge, TN 37831

Telephone: (865) 576-8401
Facsimile: (865) 576-5728
E-Mail: reports@adonis.osti.gov
Online ordering: http://www.doe.gov/bridge

Available to the public from
U.S. Department of Commerce
National Technical Information Service
5285 Port Royal Rd
Springfield, VA 22161

Telephone: (800) 553-6847
Facsimile: (703) 605-6900
E-Mail: orders@ntis.fedworld.gov
Online order: http://www.ntis.gov/help/ordermethods.asp?loc=7-4-0#online

SAND2006-7779
Unlimited Release
Printed February 2007

Helium Bubble Linkage and the Transition to Rapid He Release in Aging Pd Tritide

D. F. Cowgill
Analytical Materials Science Dept.

Sandia National Laboratories
Livermore, CA
94551-0969

Abstract

A model is presented for the linking of helium bubbles growing in aging metal tritides. Stresses created by neighboring bubbles are found to produce bubble growth toward coalescence. This process is interrupted by the fracture of ligaments between bubble arrays. The condition for ligament fracture percolates through the material to reach external surfaces, leading to material micro-cracking and the release of helium within the linked-bubble cluster. A comparison of pure coalescence and pure fracture mechanisms shows the critical He/M concentration for bubble linkage is not strongly dependent on details of the linkage process. The combined stress-directed growth and fracture process produces predictions for the onset of rapid He release and the He emission rate. Transition to this rapid release state is determined from the physical size of the linked-bubble clusters, which is calculated from dimensional invariants in classical percolation theory. The result is a transition that depends on material dimensions. The onset of bubble linkage and rapid He release are found to be quite sensitive to the bubble spacing distribution, which is log-normal for bubbles nucleated by self-trapping.

Acknowledgements

The author is indebted to Sandia colleagues for their support of this research, particularly to G. Cook Story for his strong, continued interest. This work was supported by the US Department of Energy under contract DE-AC04-94AL85000.

Contents

List of Figures

Helium Bubble Linkage and the Transition to Rapid He Release in Aging Pd Tritide

1. Introduction

Helium bubble evolution within aging metal tritides begins with a short-term bubble nucleation process [1]. The helium atoms created by beta-decay occupy interstitial sites and are mobile [2-5] at room temperature. They produce distortion of the metal lattice, which causes them to cluster and self-trap in the local expansion produced by neighboring He. According to Wilson *et al.* [6] when the clusters reach a critical size (5-6 He), they force the ejection a metal atom, forming the nucleus of a stable He bubble. Bubble nucleation begins as soon as the mobile He/Metal concentration (He/M) reaches a few atomic parts per million (appm), then decreases as the concentration of bubble surface sites becomes sufficient to provide sinks for newly-generated He. For metal hydrides (tritides) with tritium concentrations greater that a few atomic percent, this bubble nucleation stage is completed within a few days [1].

Helium-3 nuclear magnetic resonance data for Pd tritide shows that early in life, a significant fraction of the He within the small bubbles is in the high-pressure solid state [7,8]. Analysis of the melting transition of He within the bubbles for samples of several ages found a distribution of He densities consistent with a constant distribution in bubble spacing during bubble growth [1]. Thus, after nucleation, each bubble grows according to the tritium source volume supplying helium to the bubble. The small, high-pressure bubbles generate large stresses in the surrounding material. In metal tritides, the lattice atoms are displaced by a prismatic dislocation loop punching process [9-12]. With continued growth, the bubble stress fields interact, assisting the growth process and lowering the loop-punching pressure [1]. Stress in the ligament between bubbles increases as the ligament size decreases, until the stress exceeds the material's fracture strength.

This paper examines the physics leading to bubble linkage and the release of helium within the fracture network. It follows percolation of the linkage condition over arrays of neighboring bubbles and determines a He/M concentration for bulk material fracture and the transition to "rapid helium release". It also investigates the sensitivity of the bubble spacing distribution to this linkage process. In the analysis, it is assumed that the processes describing bubble linkage and inter-bubble fracture can be modeled using only "like-bubble" interactions; that is, interactions between bubbles of the same size. Effects of the bubble spacing distribution are then included using ensemble averages; i.e., by integrating over an ensemble of materials with bubble spacings (and sizes) weighted by the distribution. One aspect of the interactions between bubbles of different sizes is added through the consideration of stress-directed bubble growth, which occurs only in mixed bubble size geometries. Lastly, the effects of two very different bubble linkage processes are compared: inter-bubble ligament fracture and bubble coalescence by stress-directed bubble growth. The latter contains no fracture and is included to examine the sensitivity of the onset of rapid He release to details of the bubble linkage process.

This Page Intentionally Left Blank.

2. Stress-Directed Bubble Growth

The linkage process is modeled by first considering how a bubble's growth is influenced by the presence of a neighboring bubble. For the pair of bubbles, the maximum shear stress occurs on each bubble's surface closest to their neighbor; i.e., at the intersection with the axis interconnecting the bubble centers. As described in [1], this shear stress enhancement reduces the bubble pressure required for initiation of a dislocation loop. For two identical bubbles of radius r, pressure p, and spacing 2s, it was shown that the shear at adjacent bubble surfaces is enhanced over the shear for isolated bubbles $\tau = 3p/4$ by the factor

$$\varepsilon = [\alpha/(2-\alpha)]^3, \tag{1}$$

where $\alpha = r/s$. The bubble pressure for stress-assisted (SA) loop punching is described by [1]

$$p_{SA} = 2\gamma/r + (\mu b/r)/(1+\varepsilon), \tag{2}$$

where γ is the surface energy, μ is the shear modulus, and b is the Burgers' vector of the tritide. This enhancement becomes substantial when the bubble diameter becomes a significant fraction of the inter-bubble (center-to-center) spacing. It ultimately results in a reduction in the He/metal atom ratio required for the onset of inter-bubble fracture.

At the points on adjacent bubble surfaces where loop initiation occurs, metal atoms are displaced as members of the dislocation loops. The situation is depicted schematically by the inset in Figure 1. For the two bubbles, there are at least three Burger's vectors satisfying the loop-punching requirement. Since lattice atoms near these sites are always involved in the loop-punching process, material is preferentially removed from this region between the bubbles, relative to the regions on the opposite sides of the bubbles. This causes the bubble centers to offset closer together as they grow. With continued growth, the two bubbles will eventually coalesce. This is an athermal coalescence process and differs from thermally-activated coalescence where metal atoms migrate around bubble surfaces causing their centroids to move. Nevertheless, temperature plays a role since the probability of this stress-directed (SD) growth depends on the magnitude of the stress energy enhancement relative to the thermal energy leading to random growth.

Stress-directed bubble growth and coalescence can be modeled by noting the probability of loop initiation at a particular site on the bubble surface is proportional to $1-\exp(-\delta E/kT)$, where δE energy difference associated with the location. At ambient temperatures where $\delta E \ll kT$ the probability is proportional to δE or to the shear stress enhancement at the site. For two bubbles with centers spaced by 2s, the condition for a stress-directed growth event is

$$ds = -\varepsilon\, dr. \tag{3}$$

When $\varepsilon = 0$, the growth is random and $ds = 0$; whereas when $\varepsilon = 1$, the growth is completely directed with $ds = - dr$. That is, a growth of dr for each bubble, decreases the spacing 2s by 2dr. Inserting (1) into (3) with $dr = \alpha ds + s d\alpha$ and separating variables produces the equation

$$ds/s = - \{\alpha^3/[(2-\alpha)^3 + \alpha^4]\}\, d\alpha. \qquad (4)$$

This equation can be integrated numerically to give r_{MAX}= 0.892 R at α = 1, where 2R is the initial spacing between the bubble centers. The change in bubble spacing with bubble growth is shown graphically as a function of α in Figure 1. At small α, the half-spacing s decreases slowly from R with increasing r. As α approaches 1, s decreases more rapidly, becoming equal to r at coalescence.

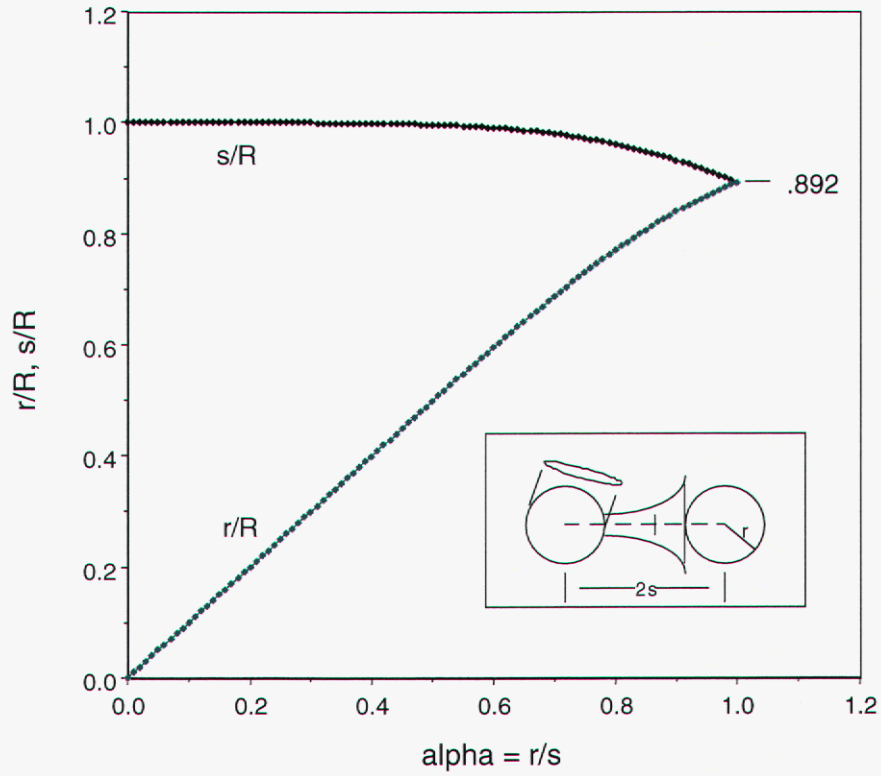

Figure 1. Stress-directed bubble growth showing coalescence at r=.892 R, if not interrupted by inter-bubble ligament fracture. Inset depicts stress contributed by a neighboring bubble assists initiation of dislocation loops.

This stress-directed growth occurs only in non-symmetric bubble geometries where the bubbles are unequally spaced. In [1], analysis of the ^{3}He NMR data on aged Pd tritide samples of various ages concluded each had a distribution in bubble pressures, implying a distribution in bubble sizes. Using the growth relations, the analysis determined that the observed pressure/size distribution was consistent with a distribution in the bubble spacing that remained constant during bubble growth. The slight motion of bubble centers described above does not significantly alter this spacing distribution, even near coalescence.

3. Inter-Bubble Fracture

In [1] an average condition for inter-bubble (IB) ligament fracture was derived using the average, three-bubble array. Following Evans [13], the average tensile stress across the triangular metal ligament between bubbles was compared with the ligament's theoretical fracture strength for a defect-free lattice. It was argued that fracture occurs when the ligament tension exceeds its fracture strength. This condition assumes the surrounding lattice material provides no support for the ligament, which is true if the material around the bubble array fractures simultaneously. This condition should apply when the calculation is performed using the mean bubble density n_B.

The Evans criterion gives the average bubble pressure for ligament fracture as

$$< p_{IBF} > = 2\gamma/r + \sigma_F [(\pi r^2 n_B^{2/3})^{-1} - 1], \quad (5)$$

where σ_F is the tritide's theoretical fracture strength. The initial average bubble spacing $2R_{AV}$ is related to the mean bubble density by $(4/3)\pi R_{AV}^3 n_B = f_P$, where the bubble packing fraction f_P=.64 is used for a random geometry [14].

Equating the pressure for stress-assisted loop punching (2) with the pressure for inter-bubble fracture (5) produces an expression for the bubble radius at IB-fracture. The fracture condition is satisfied when

$$r_{IBF} = (\mu b/\sigma_F) / [(1+\varepsilon)(1.114/\alpha^2 - 1)]. \quad (6)$$

The age or He/M atom ratio when this occurs is given by

$$He/M = (f_P/n_{MH} v_A)(r_{IBF}/R)^3. \quad (7)$$

Here n_{MH} is the metal atom density within the metal hydride phase and v_A is the He atomic volume within the bubble, which increases with age according to the bulk He equation of state [15]. At room temperature,

$$v_A (Å^3) = 18.572\, p^{-1/3} - 7.101\, p^{-2/3} + 5.375\, p^{-1}, \quad (8)$$

with p(GPa). For the pressure range found here, the first term dominates and v_A is approximately proportional to $p^{-1/3}$.

This Page Intentionally Left Blank.

4. Stress-Directed Growth to Inter-Bubble Fracture

Bubble linking can be described by the combined process of stress-assisted bubble growth to inter-bubble ligament fracture. Superposition of the stress components for the three-bubble array shows that the peak shear on each bubble's surface occurs near the points facing the neighboring bubbles. Thus, growth of 3-bubble clusters is similar to bubble pair growth, except that the growth direction is shared between the directions of the two neighbors. For three like-bubbles, Eq. (3) becomes

$$ds = -(3/4)\varepsilon\, dr, \tag{9}$$

which gives

$$ds/s = -\{\alpha^3/[(4/3)(2-\alpha)^3 + \alpha^4]\}\, d\alpha. \tag{10}$$

Without ligament fracture, 3-bubble coalescence would occur when $\alpha=1$ or $r_{MAX}=0.914$ R. However, it is shown below that the condition for r_{IBF}, given by Eq. (6), is satisfied. before r_{MAX} is reached.

4.1 Bubble Linking in Palladium Tritide

The He/M concentration for IB-fracture, for pair and 3-bubble coalescence, and for the combined SD-growth to IB-fracture process are plotted as a function of the initial bubble spacing for Pd tritide in Figure 2 . The parameters used for this calculation were taken from [1]: $n_{MH}=.06098$ Å^{-3} , b=2.846 Å , γ=15.4 GPa-Å , μ=33.6 GPa , and σ_F=2.8 GPa. The curves show that the bubble spacing dependence for the individual linkage processes differ markedly. Fracture begins with small, closely-spaced bubbles (small R), then incorporates those with large R as the He/M increases; whereas bubble coalescence starts with large, widely-spaced bubbles. The latter is a consequence of the fact that r/R is greater for large bubbles of the same age due to their lower bubble pressure and He density.

For a material with a distribution in bubble spacing, the fraction of He atoms involved in linkage increases with age (He/M) as the condition incorporates additional bubbles. The bubble spacing distribution deduced from NMR observation of the ^{3}He melting transition within the bubbles [1] is shown by the dashed line in Figure 2. Here, the number of bubbles with source radius between R and R+dR or $dN_B(R)/dR=F(R)$ is described by the 3-parameter log-normal function

$$F(R) = \exp\{-(\ln[(R-R_0)/m])^2/2\sigma_R^2\} / [(2\pi)^{1/2}(R-R_0)\sigma_R], \tag{11}$$

where R_0=30Å, m=11, and σ_R=1.14 are the location, scale, and shape parameters, respectively. While the plot shows that most of the bubbles have source radius in the range 30-50 Å, the fewer large source bubbles contain large quantities of helium. NMR found the range of the distribution was limited to 30≤R≤92 Å. The mean bubble spacing for this distribution with unlimited range is R_0+ m $\exp(\sigma_R^2/2)$ or 51.0 Å; compared to the numerical integration over the distribution with the limits 30≤R≤92 Å, which gives 45.0 Å. These mean spacings correspond

to average bubble densities of 1.1-1.7 x10^{18} bubbles/cm^3, which can be compared with TEM measurements of 0.5-1.0 x10^{18} bubbles/cm^3 observed by Thomas and Mintz [16] and the somewhat larger values of 3-10 x10^{18} bubbles/cm^3 reported by Thiebaut *et al* [17].

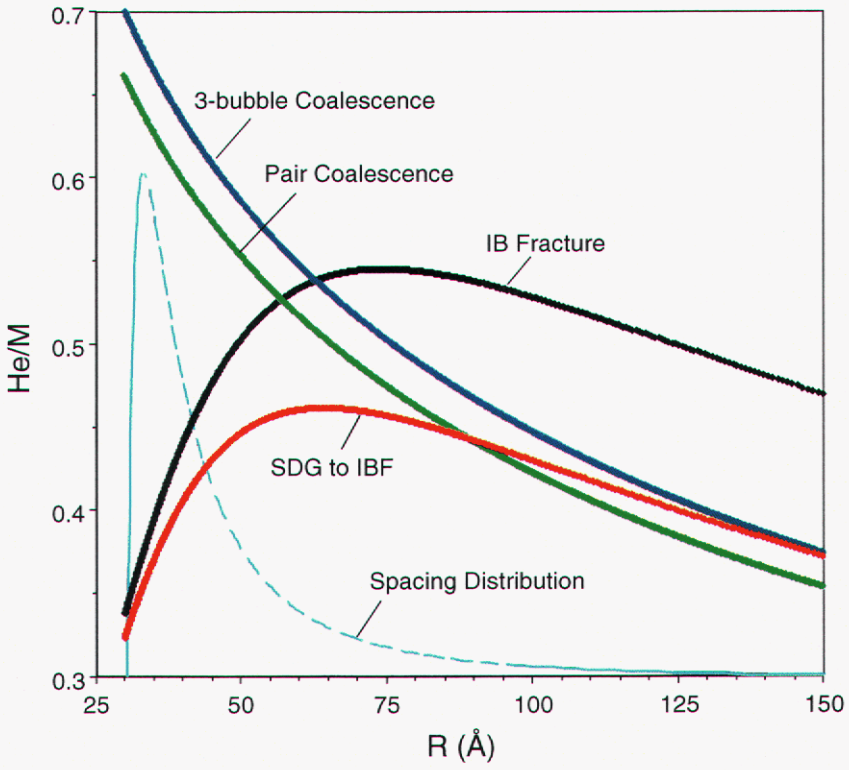

Figure 2. Critical He/M concentration for bubble linkage by pair and 3-bubble coalescence, by inter-bubble ligament fracture, and by the combined SDG-IBF mechanism as a function of the bubble center-to-center spacing 2R. The spacing distribution deduced from NMR is overlaid for reference.

Integration of the source volumes $(4/3)\pi R^3/f_P$ of bubbles satisfying the IB-fracture condition ($r \geq r_{IBF}$) over the bubble spacing distribution provides a measure of the fraction of material (or He atoms) involved. The volume fraction satisfying the IB-fracture condition, given by

$$V_{IBF} = \int [R(r \geq r_{IBF})]^3 F(R)dR \,/\, \int R^3 F(R)dR, \qquad (12)$$

is plotted in Figure 3. Similarly, the material fraction experiencing bubble pair coalescence is also shown, where the linked-bubble network is imagined as formed through coalescence by considering linked-pairs as larger single bubbles further linking with neighbors within an evolving spacing distribution. These two very different mechanisms produce an onset for bubble linkage within the range 0.34-.44 He/M. The combined process, SD-growth to IB-

fracture, results in linkage onset at the slightly lower concentration 0.32 He/M. It begins with small, closely spaced bubbles, but incorporates linkage between larger bubbles around 0.44 He/M, causing an abrupt increase in the linked fraction.

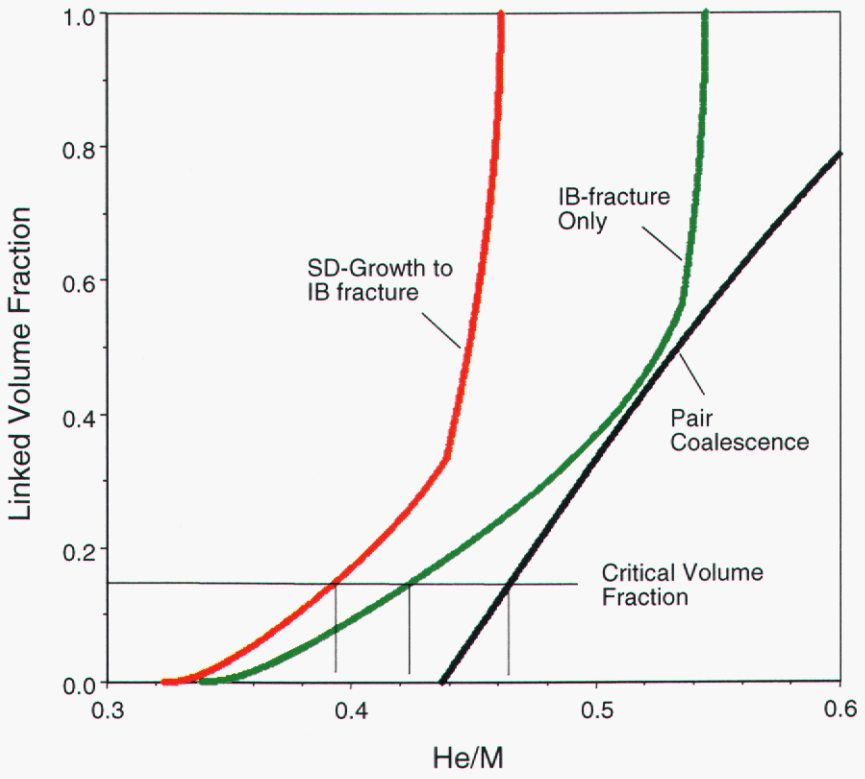

Figure 3. **Growth of the linked volume fraction (linked He atom fraction) with generated He/M, showing inclusion of stress-directed bubble growth reduces the He/M for inter-bubble fracture. Linkage by growth-produced pair coalescence would occur at only a slightly higher He/M.**

This Page Intentionally Left Blank.

5. Percolation of the Linkage Condition and Rapid Helium Release

When the fracture condition is satisfied over sufficiently extensive regions (relative to the material dimensions) or when it intersects the material surface, micro-cracking is expected to occur, causing helium release. Since the high-pressure bubbles place the metal lattice in tension, local nano-cracking between individual bubbles or small clusters may occur earlier, as described by the fracture condition, or it may be suppressed by support from the surrounding lattice. Figure 3 gives the material volume fraction satisfying the fracture condition for small, 3-bubble arrays of identical bubbles, an approximation to the fully homogeneous mixture of bubble spacings. For coalescence, the figure describes the material fraction involved in bubble pairing.

The physical extent of the linkage condition can be calculated from this volume fraction using dimensional invariants in classical percolation theory [18]. Here bubble source volumes are considered as points on an irregular 3-dimensional grid, which are linked to neighbors with probability q. The fraction of points linked is also given by $0 \leq q \leq 1$. The size of linked-clusters increases with increasing q up to the percolation threshold $q=q_C$, where the clusters become infinite. Associated with this threshold is a critical volume fraction V_C which is a dimensional invariant, independent of the array geometry. In 3-dimensions, $V_C=0.15$ [18], corresponding to 15 percent of the source volume being linked. This 15 percent level is shown in Fig. 3. Its intersection with the curves for IB-fracture and coalescence occurs at 0.42 and 0.46 He/M, respectively.

The best estimate for the onset of micro-cracking is given by the combined process, which predicts inter-connected clusters of infinite size at 0.39 He/M. At this point 15% of the helium generated within the metal or 0.06 He/M is involved. This predicted critical concentration is somewhat lower than the 0.46 He/M [19] to 0.54 He/M [20] reported for rapid release from large particle Pd tritide powders. Thus, although the condition for linked-bubble clusters has infinite extent, these data suggest the surrounding lattice may still provide sufficient support to prevent extended micro-fracture by a tortuous fracture path. Micro-fracture at a slightly higher concentration would possess a less-tortuous fracture path.

After the onset of rapid release, He is emitted at a rate determined by the slope of Fig. 3. An increase of δ(He/M)=.01 increases the linked material fraction by $\delta V \approx .033$. Since this volume fraction contains about 0.4 He/M, the amount of He emitted is about (.033)(.4)=.012 He/M. Thus in this early stage of rapid release, He is emitted at 1.2 times generation rate. This rate increases significantly around 0.44 generated He/M, as larger bubbles become incorporated into the linked network. For the pair coalescence mechanism, the emission rate would be a factor of two higher or 2.3 times the generation rate. The published data extracted Emig et al. [20] for tritium-replenished samples No. 3 and No. 5 near the beginning of rapid release give an emission rate of about 4 times the generation rate. A delay of the onset of rapid release, as the linkage condition continues to percolate, will cause the eventual emission rate to increase significantly over that predicted here.

Some helium is released from the finite clusters of linked-bubbles that intersect the surface prior to the percolation threshold. This release can be significant for small particle or thin film material. It can be calculated from the fraction of linked-material within a surface layer whose thickness equals the size (dimension) d_C of the average cluster. This size can be deduced from two other dimensional invariants. For $q<q_C$, the number of points z in the average cluster is proportional to $1/(q_C-q)^{j+1}$, where the dimensional invariant j=11/16 in 3-dimensions. Also, z is proportional to d_C^D, where D=2.5 is the fractal dimension [21]. Thus, the layer thickness d_C is proportional to $(q_C-q)^{-.675}$. This thickness can be put on an absolute basis by noting that large source volumes can be considered as clusters of the smallest; i.e., the source volume with $R=R_0$, which defines the separation between the z points. Then $q=V/f_P$ and $q_C=V_C/f_P=0.234$. The proportionality constant can be evaluated for q=0 where $d_C=2R_0$, giving

$$d_C(\text{Å}) = 16.67 / (V_C-V)^{.675} \tag{11}$$

for the thickness of the releasing layer.

The fractional helium release is the fraction of the total particle volume determined by the linked volume fraction within the surface layer of thickness d_C. For spherical particles with radius R_P, the fractional release is given by

$$V_P = V\,[1 - (1 - d_C/R_P)^3] \tag{12}$$

and for thin films with thickness L, $V_F=Vd_C/L$. Figure 4 gives a plot of the fractional He release for spherical powder particles of several diameters $2R_P$. For powder particles 5 micron diameter and larger, the onset is quite abrupt at 0.39 He/M, while 0.5 micron powders show an increase to 10 percent release at 0.38 He/M. These surfaces also contribute the low level early He release throughout aging, as described in [1]. For the 0.5 μm $PdT_{.65}$ powder, this early release fraction was calculated to be about 5 percent of the generated He. Thus the total quantity of released helium doubles at 0.38 He/M. The slope of the 0.5 micron curve at this point yields an instantaneous He release rate of about 1.2 times the generation rate.

The plots in Fig. 4 are merely volume fractions and do not include near-surface modifications of the bubble spacing or its distribution. They were calculated using the bubble density and spacing distribution determined within the bulk. At 0.10 volume fraction, d_C=86 Å for the 0.5 micron diameter powder. This thickness is only a factor of two greater than the He escape depth λ_{esc}=40 Å [1], the strongly modified near-surface region producing the early release. Thus the plots somewhat underestimate the size of clusters needed to link this fraction of He to the surface. A more accurate calculation would require information on how the bubble spacing distribution is modified in this near-surface region.

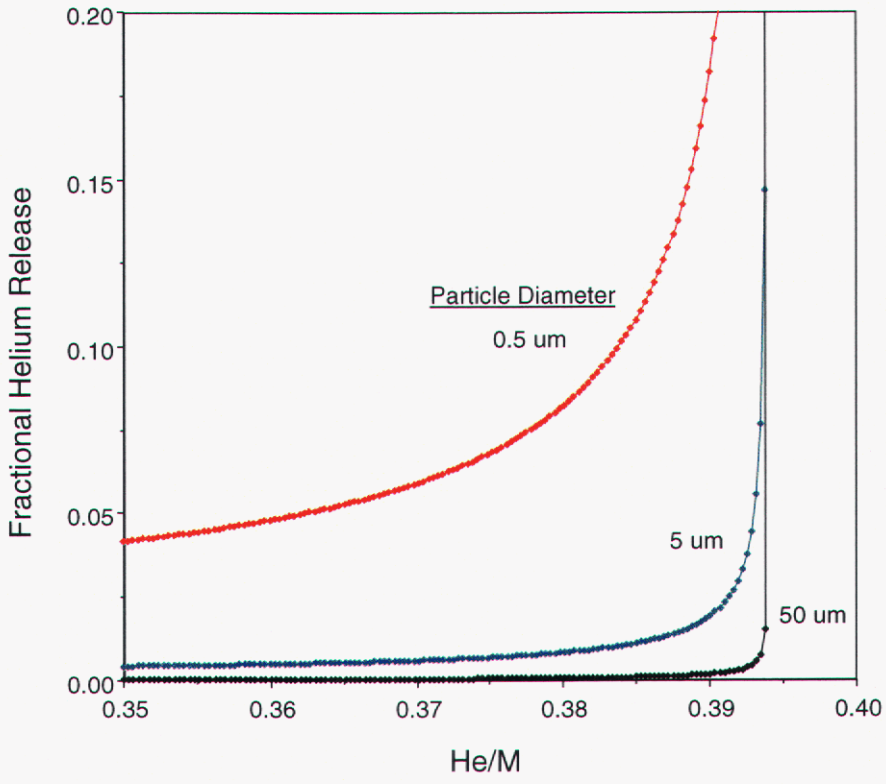

Figure 4. Fractional He release from percolation of surface-connected linked-bubble clusters for Pd tritide powder particles 50, 5, and 0.5 μm diameter. Small particles show a significant release at an earlier age.

Sensitivity of the linkage process to the bubble spacing and its distribution can be examined by varying the distribution and determining its effect on the linked volume fraction. Figure 5 shows an example of a small change: the effect of truncating the distribution at an arbitrary 164 Å compared to the NMR-deduced 92 Å, where both distributions are normalized. The very few larger bubbles included by this change contain a significant quantity of He, helium that becomes part of the linked fraction at an early age. The nucleation dynamics which create the deduced truncation are not well understood. Similarly, a factor of two increase in the bubble density, created using R_0=19.5 Å, produces an even more dramatic effect. Thus it is clear that the onset and development of the bubble linkage depends strongly on the bubble spacing and details of its distribution.

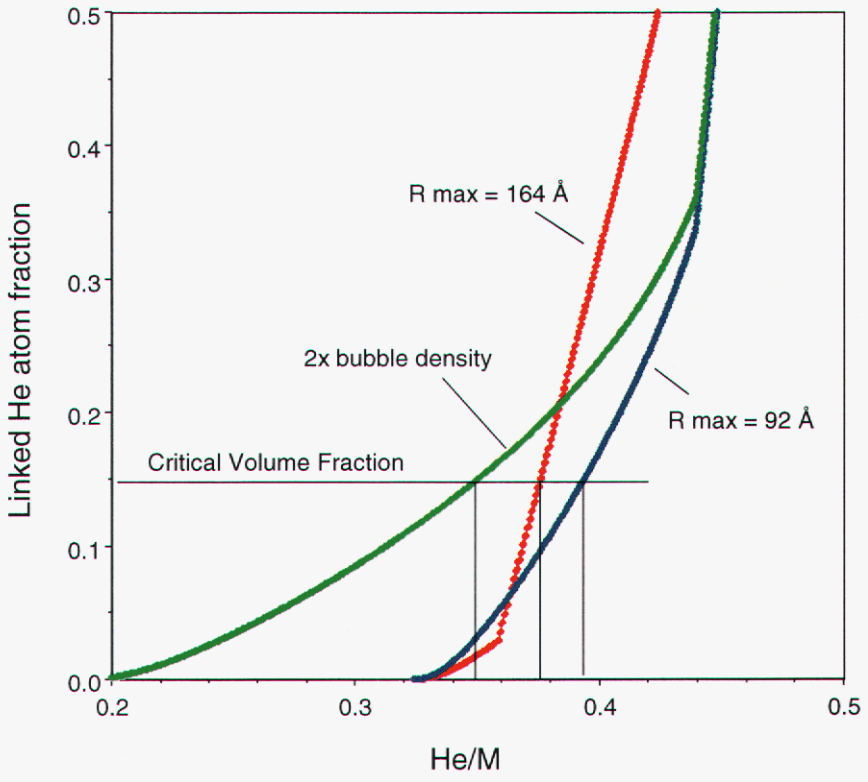

Figure 5. **A comparison of the linked volume fraction for a bubble spacing distribution with R_{max}=164 Å, compared to the NMR-deduced distribution with R_{max}=92 Å, showing sensitivity to the distribution. The effect of doubling the bubble density is also shown.**

6. Discussion and Conclusions

The physics of bubble growth and inter-bubble fracture in aging metal tritides has been examined. Two different bubble linkage mechanisms were presented: Coalescence by stress-directed bubble growth (SDG) and linkage by inter-bubble ligament fracture (IBF). It is found for Pd tritide that IBF produces an onset of bubble linkage around 0.34 He/M, beginning with large well-spaced bubbles; while SDG would cause bubble coalescence to start at 0.44 He/M with small closely-spaced bubbles, provided fracture doesn't occur. The combined mechanism, SDG-to-IBF gives the best estimate for linkage onset around 0.32 He/M, beginning with large bubbles.

Growth of the linked-bubble clusters is modeled using classical percolation theory. Here bubbles are considered "linked" if the fracture criterion is satisfied locally. In the bulk, actual micro-fracture likely occurs only when the fracture condition is sufficiently wide-spread that the surrounding lattice provides no support. It is found that the two very different linkage mechanisms produce percolating clusters of infinite size at nearly the same age of 0.44±.02 He/M, suggesting an insensitivity to details of the linkage process. A previous calculation also found a low sensitivity to material fracture strength: a 30% increase in the fracture strength produced only a 10% increase in the critical He/M [1]. The combined SDG-to-IBF linkage process is found to produce infinite clusters at 0.39 He/M.

For small particle powders or thin films, a significant fraction of the linked-bubble clusters intersect the surface prior to infinite cluster percolation. The physical extent of the clusters as deduced from percolation theory provides a thickness dimension to the releasing layer. The model produces a reduction in the apparent He/M for the onset of rapid He release that depends on particle size.

The model presented here considers nearest-neighbor, "like-bubble" interactions only; i.e., interactions between bubbles of the same size and shape. Further work on modeling could examine stress-assisted and stress-directed growth for unlike bubbles, using complex averages over the spacing distribution. Since cluster sizes are deduced from percolation of the inter-bubble fracture condition, which relies only on the linked-volume fraction, the percolation approach should remain applicable. However, consideration of the sensitivity of bubble linkage to the bubble spacing finds that He retention is controlled primarily by the nucleated bubble spacing distribution. Small changes in this distribution were found to produce significant effects on the onset of rapid He release. This distribution may be difficult to know with sufficient detail to warrant significant improvements in the fidelity of the He release model. Conversely, limitations on the ability to control this distribution and the effects of bubble nucleation at impurities will likely produce a limit on the control of He release behavior.

This Page Intentionally Left Blank.

References

[1] D.F. Cowgill, "Helium Nano-Bubble Evolution in Aging Metal Tritides", Technical Report SAND2004-1739, Sandia National Laboratories, May 2004.

[2] G.J. Thomas, W.A. Swansiger, and M.I. Baskes, J. Appl Phys 50 (1979) 6942.

[3] G.J. Thomas and R. Bastasz, J. Appl. Phys. 52 (1981) 6426.

[4] T. Wichert, M. Deicher, G. Grubel, E. Recknagel, and W. Reiner, Phys. Rev. Letters 55 (1985) 726.

[5] C.G. Chen and H.K. Birnbaum, J. Nucl. Mater. 79 (1979) 128.

[6] W.D. Wilson, C.L. Bisson and M.I. Baskes, Phys. Rev. B 24 (1981) 5616.

[7] G.C. Abell and A. Attalla, Phys. Rev. Lett. 59 (1987) 995; Fusion Tech. 14 (1988) 643.

[8] G.C. Abell and D.F. Cowgill, Phys. Rev. B 44 (1991) 4178.

[9] G.W. Greenwood, A.J.E. Foreman, and D.E. Rimmer, J. Nucl. Mater. 4 (1959) 305.

[10] W.G. Wolfer, Phil. Mag. A 58 (1989) 285; A 59 (1989) 87.

[11] H. Trinkaus, Radiat. Eff. 78 (1983) 189.

[12] S.E. Donnelly, Radiat. Eff. 90 (1985) 1.

[13] J.H. Evans, J. Nucl. Mater. 68 (1977) 129 and 76-7 (1978) 228.

[14] M.F. Wehner and W.G. Wolfer, J. Statistical Phys. 42 (1986) 509.

[15] R.L. Mills, D.H. Liebenberg, and J.C. Bronson, Phys. Rev. B 21 (1980) 5137.

[16] G.J. Thomas and J.M. Mintz, J. Nucl. Mater. 116 (1983) 336.

[17] S. Thiebaut, B. Decamps, J.M. Penisson, B Limacher, and A. Percheron Guegan, J. Nucl. Mater. 277 (2000) 217.

[18] V.K.S. Shante and S. Kirkpatrick, Adv. Phys. 20 (1971) 325.

[19] G.C. Abell, L.K. Matson, R.H. Steinmeyer, R.C. Bowman Jr., and B.M. Oliver, Phys. Rev. B41 (1990) 1220.

[20] J.A. Emig, R.G. Garza, L.D. Christensen, P.R. Coronado, and P.C. Souers, J. Nucl. Mater. 187 (1992) 209.

[21] D. Stauffer and A. Aharony, "Introduction to Percolation Theory", 2nd Ed. (Taylor and Francis, London, 1992) 61.

This Page Intentionally Left Blank.

Distribution

External:

1 Los Alamos National Laboratories
c/o Ken Keeler
P.O. Box 1663, C934
Los Alamos, NM 87545

1 Los Alamos National Laboratories
c/o Burt Davis
P.O. Box 1663, G780
Los Alamos, NM 87545

1 Los Alamos National Laboratories
c/o James Peery
P.O. Box 1663
Los Alamos, NM 87545

1 Los Alamos National Laboratories
c/o David Lohmeier
P.O. Box 1663
Los Alamos, NM 87545

1 Los Alamos National Laboratory
c/o Brad Meyer
500B, Bldg. C934
Los Alamos, NM 87545

1 Los Alamos National Laboratory
c/o Kevin Honnell
500B, Bldg. C934
Los Alamos, NM 87545

1 Savannah River National Laboratory
c/o Paul Cloessner
Bldg. 773-A
Aiken, SC 29808

1 Savannah River National Laboratory
c/o Scott West
Bldg. 773-42A
Aiken, SC 29808

External (continued):

1 Savannah River National Laboratory
c/o Dennis Fish
Bldg. 773-A
Aiken, SC 29808

1 Savannah River National Laboratory
c/o Steven Wyrick
Bldg. 773-A
Aiken, SC 29808

1 Lawrence Livermore National Laboratory
c/o Adam Schwartz
Bldg. L-353
Livermore, CA 94551

1 Lawrence Livermore National Laboratory
c/o Kris Winer
Bldg. L-170
Livermore, CA 94551

1 Lawrence Livermore National Laboratory
c/o Wilhelm Wolfer
Bldg. L-353
Livermore, CA 94551

1 Lawrence Livermore National Laboratory
c/o Christopher Krenn
Bldg. L-353
Livermore, CA 94551

1 Pacific Northwest National Laboratory
c/o David Gelles
P.O. Box 999
Richland, WA 99352

Internal:

1	MS0335	Clark Snow, 2725
1	MS0521	Frank Bacon, 2724
1		Jaime Moya, 0521
1	MS0867	James Browning, 2725
1	MS0869	Len Beavis, 2722
1	MS0885	Dick Salzbrenner, 1820
1	MS0886	Paul Kotula, 1822
1	MS1056	Barney Doyle, 1111
1	MS1146	Patrick Griffin, 1384
1		Philip Cooper, 1384
1	MS1231	Robert Spulak, 5042
1	MS1322	John Aidun, 1435
1	MS1411	Jeff Hoyt, 1814
1		Stephen Foiles, 1814
1	MS9004	Jill Hruby, 8100
1		Brian Damkroger, 8130
1	MS9007	Rena Zurn, 8205
1		Robert Monson, 8244
1		Tony Lajeunesse, 8205
1	MS9014	Jim Harrison, 8241
1	MS9035	Chuck Cadden, 8220
1		Carl Pretzel, 8224
1		Steve Robinson, 8224
1		G. Cook Story, 8224
1		Steve Rice, 8224
1	MS9042	Tony Chen, 8776
1		Jonathan Zimmerman, 8776
1	MS9102	Russ Miller, 8230
1	MS9151	Chuck Oien, 8940
1	MS9153	Doug Henson, 8800
1	MS9159	Mike Hardwick, 8964
1	MS9221	Ed Cull, 8510
1	MS9402	Rion Causey, 8758
10		Don Cowgill, 8758
1		Kristin Hertz, 8772
1		Dean Buchenauer, 8758
1		Arlyn Antolak, 8772
1		Eric Majzoub, 8755
2	MS0899	Technical Library, 4536
2	MS9018	Central Technical Files, 8944